Incorporating a semi-Lagrangian body-free-surface intersection point in a fully nonlinear potential flow model

Jacob Hicks[1], Harry Bingham[1], Robert Read[1], and Allan P. Engsig-Karup[2]

[1] Department of Mechanical Engineering

[2] Department of Applied Mathematics and Computer Science

Technical University of Denmark, 2800 Kgs. Lyngby, Denmark

jabhh@mek.dtu.dk, hbb@mek.dtu.dk, rrea@mek.dtu.dk, apek@dtu.dk

Introduction

This abstract presents our progress in the development of a fully nonlinear potential flow solver capable of modelling wave-structure and wave-bottom interactions. The numerical method is based on a finite difference method with a σ-transform in the vertical direction, as presented in Bingham and Zhang (2007), and boundary conditions are imposed in a robust way as described in Engsig-Karup et al. (2009). Wave-structure interaction is implemented using the Immersed Boundary Method (IBM) shown in Kontos et al. (2016), where the body boundary condition is satisfied by a Weighted Least Squares approximation, as described in Lindberg et al. (2014). The current work details the introduction of a semi-Lagrangian point tracking the body-free-surface intersection, which improves robustness and extends the capabilities of the solver to increasingly nonlinear wave-structure interaction. The accuracy and convergence of the scheme are validated by comparison with the second-order wave generation theory of Schäffer (1996).

Formulation

The problem is defined in terms of the velocity potential ϕ, and can be expressed in terms of a moving frame of reference with velocity U. This is necessary if forward motion of a ship is to be considered. In the general (3D) case, a Cartesian coordinate system $(\mathbf{x}, z) = (x, y, z)$ is defined with the z-axis directed vertically upward from the mean water level at $z = 0$, and the x-axis aligned with the direction of forward motion. The initial-boundary-value problem is defined by

$$\nabla^2 \phi + \phi_{zz} = 0, \qquad \text{in } \Omega, \qquad (1)$$

$$\eta_t + \nabla\eta(\nabla\tilde{\phi} - \tilde{w}\nabla\eta - \mathbf{U}) = \tilde{w}, \qquad \text{on } z = \eta, \qquad (2)$$

$$\tilde{\phi}_t + \nabla\tilde{\phi}\left(\frac{1}{2}\nabla\tilde{\phi} - \mathbf{U}\right) - \frac{1}{2}\tilde{w}^2(1 + \nabla^2\eta) = -g\eta, \qquad \text{on } z = \eta, \qquad (3)$$

$$\phi_z + \nabla h \nabla \phi = 0, \qquad \text{on } z = -h, \qquad (4)$$

$$\phi_n = V_n, \qquad \text{on } \mathbf{S}_b, \qquad (5)$$

$$\eta(\mathbf{x}, 0), \ \tilde{\phi}(\mathbf{x}, 0) \qquad \text{given.} \qquad (6)$$

Here $\nabla = (\partial_x, \partial_y)$ is the horizontal gradient operator, $\mathbf{U} = (U, 0, 0)$ is the forward velocity vector, g is the gravitational constant, and $\mathbf{x}$ represents a horizontal vector. Equation (1) is the Laplace equation, Eq.'s (2) and (3) are the kinematic and dynamic free surface boundary conditions, respectively. These are expressed in terms of surface quantities $\tilde{\phi}(\mathbf{x}, t) = \phi(\mathbf{x}, \eta, t)$ and $\tilde{w} = \phi_z|_{z=\eta}$. Equation (4) is the impermeable bottom condition, and Eq. (5) imposes a no-flux condition through the body surface $\mathbf{S}_b$, with V_n the body velocity. In this work the initial conditions are still water, and wave motion is imposed via the moving body. Subscripts represent partial derivatives in the given direction. In the current abstract only 2D forced motion problems are considered.

Numerical Method

The efficiency of finite difference methods on structured grids is utilised by mapping the time-dependent physical domain to a time-invariant computational domain with a σ-transformation. This transformation requires a smooth and C^2-continuous free surface over the entire domain, implying that

an artificial free surface must be created in the interior of any surface-piercing body. The classical explicit four-stage, fourth-order Runge-Kutta method is used to time-step the free surface boundary conditions, and a 9th-order, 11-point Savitsky-Golay smoothing filter is applied to the free surface after every time step. A stencil size of $r = 3$ is used, giving second-order accuracy, with 70 points per wavelength in the horizontal direction and 30 points in the vertical direction. Cosine stretching in the vertical direction ensures sufficient resolution near the free surface, in accordance with Bingham and Zhang (2007).

Body-free-surface intersection

In this work, waves are generated by a paddle wavemaker. As the paddle moves freely through the computational grid, the exact position of the intersection between the body and free surface must be estimated at each time step in order to satisfy the no-flux condition through the body surface. The interior free surface is then artificially constructed by extrapolating the free surface into the body, and C^2-continuity is ensured by solving a 7th-order polynomial where η, η_x, and η_{xx} are specified at the body-free-surface intersection. To improve the robustness of this process, we implement a semi-Lagrangian particle that tracks the body-free-surface intersection at all times. There are two conditions required for such a particle: it must remain on the body surface at all times; and it must remain on the free surface at all times. In order to satisfy the first condition, the velocity of the particle, $\mathbf{V}_P$, is required to be tangential to the body surface at all times. The second condition may then be satisfied by choosing the magnitude of the velocity as described in Liu et al. (2001), namely

$$\mathbf{V}_P = \frac{(\nabla\phi_P - \mathbf{U}) \cdot n_{FS}}{e_\tau \cdot n_{FS}} e_\tau + \mathbf{U}, \tag{7}$$

where $\mathbf{U}$ is the velocity of the body at the intersection point P, e_τ is the unit tangential vector on the body surface at P, and n_{FS} is the unit normal vector to the free surface at P. For a moving body such as a wedge or paddle in forced motion, the body velocity and unit tangential vector are known at all times. The unit normal vector to the free surface may be calculated based on the current position of the intersection point and the free surface. The gradient of the velocity potential at the intersection point may be approximated by applying a Weighted Least Squares stencil of derivative operators to the surrounding fluid points. Defining the velocity of the body-free-surface intersection point by Eq. (7) allows the position of the point to be time-stepped by

$$\frac{\partial x_P}{\partial t} = V_P, \tag{8}$$

which can easily be included as an additional ODE in the current explicit four-stage Runge-Kutta procedure. The potential associated with the intersection point may then be updated by a modified dynamic free surface boundary condition; namely

$$\frac{\partial \phi_P}{\partial t} = -g\eta - \frac{1}{2}\nabla\phi_P \cdot \nabla\phi_P + V_P \cdot \nabla\phi_P. \tag{9}$$

Implementing a semi-Lagrangian point in this way allows for improved construction of the artificial interior free surface and, when mesh points exit the body, their new velocity potential and free surface elevation values may be calculated more accurately based on ϕ_P and η_P respectively.

Test cases

To test this extension we consider a wave-generation problem, where a moving body in the form of a paddle wavemaker is translated in forced motion. Both theory and experimental data describing this problem up to second order were presented in Schäffer (1996), which is the basis of our comparisons. The tested waves are collected in Table 1. All cases were run at a water depth of $h = 0.7$ m. In each case the second-order motion of the wavemaker is given by

$$X(t) = \Re\{-iX_a e^{i\omega t} - i\frac{A^2}{h}\mathscr{F}^+ e^{i(\omega_n + \omega_m)t}\}. \tag{10}$$

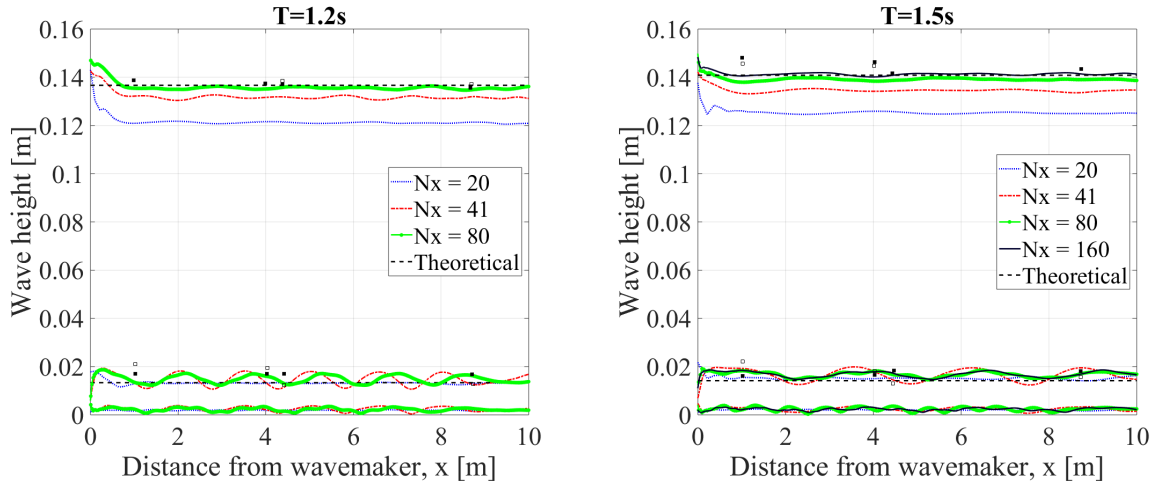| T [s]	H [m]	kh [-]	H/L [-]
1.2	0.15	2.03	0.0691
1.5	0.155	1.41	0.0497
2.0	0.12	0.95	0.0261

Table 1: Regular waves tested.

Figure 1: Harmonic analysis of waves generated by second-order theory. Different colours represent the number of points per wavelength in the horizontal.

Here X_a is the complex first-order wave amplitude found by $A = c_0 X_a$, where

$$A = \frac{h}{2}\left(\sqrt{1 + 2\frac{H}{h}} - 1\right),\tag{11}$$

and c_0 is the Biésel transfer function of Biésel (1951). The coefficient $\mathscr{F}^+$ is the superharmonic transfer function given in Schäffer (1996). For regular waves, $\omega_n = \omega_m$. The wavemaker motion is ramped up from zero over three wave periods in each simulation. The test section extends 10 m from the paddle mean position, and a sponge layer measuring 5 wavelengths absorbs the propagating waves. Once the initial ramped wave has propagated through the test section, the free surface elevation is recorded for 4 wave periods. A harmonic analysis is then carried out on the recorded time series, where third harmonics are also taken into account. Figure 1 shows the convergence of second-order wave generation for two cases. Included are data from Schäffer (1996): black squares denote experimental second-order wave generation; white squares denote first-order wave generation. The simulations were carried out at second-order accuracy ($r = 3$) and have convergence rates of 1.86, 1.78, and 2.5 in the first harmonic, for periods $T = 1.2$ s, $T = 1.5$ s, and $T = 2$ s, respectively. Errors are measured with respect to the expected theoretical primary wave amplitude. Finally, Figure 2 shows the difference between first and second order wavemaker theory for a waves with periods $T = 2$ s and $T = 2$ s.

Conclusion

A semi-Lagrangian point tracking the body-free-surface intersection has been successfully implemented in a fully nonlinear potential flow solver. Simulations of wave generation by a paddle wavemaker show satisfactory agreement with theoretical and experimental work by Schäffer (1996), using both first- and second-order wavemaker theory. Ultimately, the aim of this work is to extend the existing second-order theory to account for higher harmonics, and to develop a method of optimizing wavemaker signals to generate stable, bound waves with an arbitrary number of harmonics. In addition to this, ongoing work is aimed at extending the solver to a high-order accurate scheme.
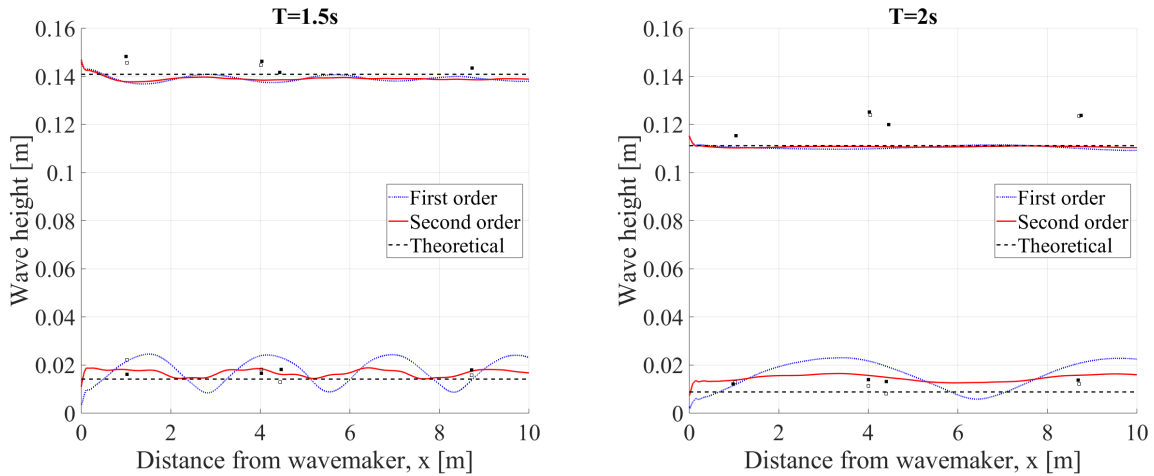
Figure 2: Comparison of first and second-order wave generation.

Acknowledgements

F. Biésel. Etude théorique d'un type d'appareil à houle. *La Houille Blanche*, 6:152–165, 1951.

H. B. Bingham and H. Zhang. On the accuracy of finite-difference solutions for nonlinear water waves. *Journal of Engineering Mathematics*, 58:211–228, 2007.

A. P. Engsig-Karup, H. B. Bingham, and O. Lindberg. An efficient flexible-order model for 2D nonlinear water waves. *Journal of Computational Physics*, 228:2100–2118, 2009.

S. Kontos, H. B. Bingham, O. Lindberg, and A. P. Engsig-Karup. A robust WENO scheme for nonlinear waves in a moving reference frame. *Journal of Hydrodynamics*, 28:482–488, 2016.

O. Lindberg, H. B. Bingham, and A. P. Engsig-Karup. Towards real time simulation of ship-ship interaction - Part III: Immersed body boundary condition and double body ship-ship interaction. In *29th International Workshop on Water Waves and Floating Bodies*, 2014.

Y. Liu, M. Xue, and D. K. P. Yue. Computations of fully nonlinear three-dimensional wave-wave and wave-body interactions. Part 2: Nonlinear waves and forces on a body. *Journal of Fluid Mechanics*, 438:41–66, 2001.

H. A. Schäffer. Second-order wavemaker theory for irregular waves. *Ocean Engineering*, 23:47–88, 1996.